

32 central system with quantum numbers of vacuum. The central system is
 33 well separated from outgoing intact protons by large rapidity gaps.

34 Despite the fact that CEP is topologically very simple, it is theoret-
 35 ically very complex and rich phenomena. The CEP includes both resonance
 36 and continuum productions. Hence, significant interference effects between
 37 resonance and continuum production are present. Furthermore, there may
 38 be significant rescattering (absorption) effects via additional interaction be-
 39 tween the protons and/or hadron and proton [4]. A generic diagram of CEP
 40 with resonance and continuum production is shown in Fig. 1.

41 The data from the Solenoidal Tracker at RHIC [5] (STAR) experiment
 42 at the Relativistic Heavy Ion Collider [3] (RHIC), gives a unique oppor-
 43 tunity to perform such studies since the DIPE is expected to be dominant
 44 CEP mechanism at RHIC energies [4]. This was confirmed by the most
 45 recent results of the CEP in proton-proton collisions at $\sqrt{s} = 200$ GeV [4].
 46 The detection of the forward-scattered protons with the measurement of
 47 the central system allows full control of the interaction's kinematics and
 48 verification of its exclusivity.

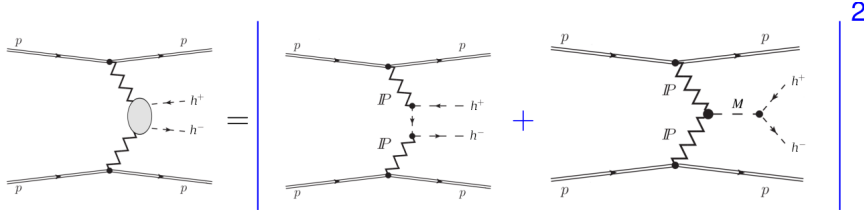


Fig. 1. A generic diagram of central exclusive production of two hadron as combination of continuum and resonance production.

49

2. Experimental setup

50 The STAR is a multi-purpose detector consisting of many sub-detectors,
 51 allowing measurement and identification of particles. In the Time Projection
 52 Chamber [6] (TPC), charged particles are tracked and their energy loss as
 53 a function of their momenta is measured in pseudorapidity range of $|\eta| < 1$
 54 and full azimuthal angle. In combination with measuring the time-of-flight
 55 information in the Time Of Flight [7] (TOF) system, the STAR detector
 56 enables precise particle identification. Forward rapidity Beam-Beam Coun-
 57 ters [8] (BBC), covering $2.1 < |\eta| < 5.0$, are used to ensure rapidity gaps.
 58 In addition, the STAR experiment has silicon strip detectors installed in
 59 Roman Pots [9] at 15.8 and 17.6 meters on both sides of the interaction
 60 point to measure protons from the CEP process. In each Roman Pot, a
 61 package of four silicon strip detectors and a scintillation trigger counter is

62 installed giving spatial resolution of $30 \mu\text{m}$ and active area of $79 \times 49 \text{ mm}^2$.
 63 The capability of measuring forward-scattered protons' transverse momenta
 64 is crucial to verify the exclusivity.

65 3. Data sample and event selection

66 In 2015 and 2017, the STAR experiment collected proton-proton collision
 67 data at $\sqrt{s} = 200$ and 510 GeV , respectively. About 622 (560) million
 68 CEP event candidates were triggered in 2017 (2015). The next paragraphs
 69 describe the selection criteria used to select a sample of CEP events at
 70 $\sqrt{s} = 510 \text{ GeV}$. The selection criteria used at $\sqrt{s} = 200 \text{ GeV}$ are similar,
 71 their detailed description can be found here [4].

72 The CEP events were triggered by requiring signals in at least one Ro-
 73 man Pot station in lower or upper branch on each side of the interaction
 74 point and requiring lack of signals in the other branches to reduce pile-up
 75 events, or events involving proton dissociation. In the TOF, 2 – 10 hits were
 76 required to ensure at least two in-time tracks in the TPC. Moreover, a veto
 77 on signals in both the BBC and the Zero Degree Calorimeter detectors was
 78 imposed to ensure the rapidity gaps characteristic to CEP events.

79 In the offline analysis, only events with exactly one forward-scattered
 80 proton, measured in Roman Pots, on each side of the interaction point were
 81 selected. This was achieved by requiring to have all eight silicon planes
 82 used in the proton reconstruction and to have transverse momenta of the
 83 scattered protons inside a fiducial region, as listed in the legend of Fig. 2
 84 (right), to ensure high geometrical acceptance and good track quality.

85 Next, the information of the central system was checked. Only events
 86 with exactly two opposite-charged TPC tracks matched with two TOF hits,
 87 originating from the same vertex, were selected. To ensure high geometrical
 88 acceptance for the central tracks in the entire fiducial phase space, further
 89 criteria were applied: a cut on the z -position of the vertex ($|z\text{-position of}$
 90 $\text{vertex}| < 80 \text{ cm}$) and a cut on pseudorapidity of central tracks ($|\eta| < 0.7$).
 91 In addition, tracks reconstructed in the TPC had to satisfy track quality
 92 cuts – number of hits used in track reconstruction (> 25) and number of
 93 hits used for determining the ionization energy loss (> 15).

94 Then, the cut on the missing transverse momentum ($p_{\text{T}}^{\text{miss}} < 100 \text{ MeV}$)
 95 was used to ensure exclusivity of the event. The $p_{\text{T}}^{\text{miss}}$ is defined as the
 96 absolute value of sum of the transverse momenta of all measured particles.
 97 Due to the conservation of the momentum, the $p_{\text{T}}^{\text{miss}}$ should be equal to zero
 98 for the CEP processes.

99 Finally, the particle identification was done based on combined informa-
 100 tion from the TPC, the ionization energy loss of the particle, and from TOF
 101 (m_{TOF}^2) [4], where the m_{TOF}^2 is the squared invariant mass of a particle type

102 (π , K , and p). After applying all the selection criteria mentioned above,
 103 62077 $\pi^+\pi^-$, 1697 K^+K^- , and 125 $p\bar{p}$ CEP event candidates were selected.

104

4. Results

105 In Fig. 2 (left), the differential cross-section for CEP of $\pi^+\pi^-$ at $\sqrt{s} =$
 106 200 GeV [4] as a function of the invariant mass of the pair is presented with
 107 Monte Carlo model predictions from Dime [11], GenEx [12] and the MBR
 108 model [13]. Since these models account for continuum production only, they
 109 are not expected to fully describe the data. Figure 2 (right) shows the in-
 110 variant mass distribution of selected $\pi^+\pi^-$ pairs at $\sqrt{s} = 510$ GeV with
 111 GRANIITTI [10] prediction. It calculates invariant mass spectra assuming
 112 both continuum and resonance contributions. Hence, it takes into account
 113 significant interference effects. In addition, significant rescattering (absorp-
 114 tion) effects via additional interaction between the protons and/or hadron-
 115 proton are also embedded. The new tune GRANIITTI v. 1.080 includes
 116 CEP resonance couplings also tuned to the STAR CEP results at $\sqrt{s} =$
 117 200 GeV [4]. The following resonances were included in the GRANIITTI cal-
 118 culation: $f_0(500)$, $\rho(770)$, $f_0(980)$, $\phi(1020)$, $f_2(1270)$, $f_0(1500)$, $f_2(1525)$,
 119 and $f_0(1710)$. The results at $\sqrt{s} = 510$ GeV were corrected for particle
 120 reconstruction efficiency in the TPC and TOF. The correction is called "ac-
 121 ceptance corrected" as the full efficiency corrections are still under study.
 122 The results were normalized such that area under the distribution is equal
 123 to one. The invariant mass distribution of $\pi^+\pi^-$ pairs shows expected fea-
 124 tures: a drop at about $m(\pi^+\pi^-) = 1$ GeV, possibly due to the quantum
 125 mechanical negative interference of $f_0(980)$ with the continuum contribu-
 126 tion, and a peak consistent with the $f_2(1270)$. Shown error bars represent
 127 the statistical uncertainties only and natural units are used.

128 Figure 3 shows the invariant mass distribution of $\pi^+\pi^-$ pairs at $\sqrt{s} =$
 129 510 GeV differentiated in two regions of $\Delta\varphi$, where different Pomeron dy-
 130 namics is expected. The $\Delta\varphi$ is the difference of azimuthal angles between
 131 the forward protons. A suppression of $f_2(1270)$ and an enhancement at low
 132 invariant mass in $\Delta\varphi < 90^\circ$ are seen. Figure 4 illustrates invariant mass
 133 distributions of selected K^+K^- and $p\bar{p}$ pairs measured within the STAR
 134 acceptance. The invariant mass of K^+K^- pairs shows a peak at about
 135 $m(K^+K^-) = 1.5$ GeV, possible $f_2(1525)$, and a strong enhancement at low
 136 invariant mass, possible $f_0(980)$ or $\phi(1020)$. The invariant mass distribu-
 137 tion of $p\bar{p}$ pairs has low statistics and does not show any resonances. In
 138 general, GRANIITTI can describe shapes of all presented distributions at
 139 $\sqrt{s} = 510$ GeV.

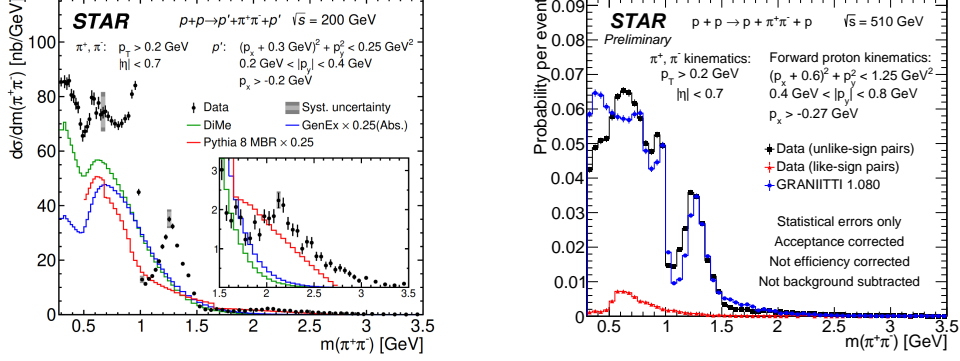


Fig. 2. Left: Differential cross-section as a function of invariant mass of $\pi^+\pi^-$ pairs at $\sqrt{s} = 200$ GeV. Right: The acceptance corrected invariant mass spectrum of exclusively produced $\pi^+\pi^-$ pairs at $\sqrt{s} = 510$ GeV.

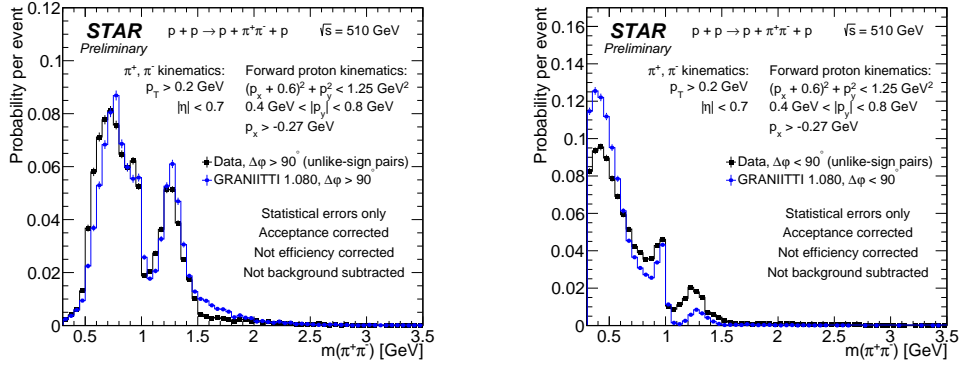


Fig. 3. Acceptance corrected invariant mass spectra of exclusively produced $\pi^+\pi^-$ pairs in two regions of the difference of azimuthal angles of the forward-scattered protons: $\Delta\phi > 90^\circ$ (left) and $\Delta\phi < 90^\circ$ (right). Error bars represent the statistical uncertainties.

140

5. Summary

141 Recent results on the CEP of $\pi^+\pi^-$, K^+K^- , and $p\bar{p}$ pairs measured
 142 with the STAR experiment in proton-proton collision at $\sqrt{s} = 200$ and
 143 510 GeV have been presented. The presented results confirm features seen
 144 in previous experiments with some new features like the peak at about
 145 $m(K^+K^-) = 1$ GeV in the distribution of K^+K^- pairs at $\sqrt{s} = 510$ GeV
 146 are observed. The new Monte Carlo event generator, GRANIITTI, is able
 147 to describe the shape of the presented data suggesting significant role of
 148 resonance production in the CEP process.

149

Acknowledgments

150 The work was supported by the Grant Agency of the Czech Technical
 151 University in Prague, grant No. SGS22/174/OHK4/3T/14 and by the Min-
 152 istry of Education, Youth and Sports of the Czech Republic through the
 153 project LM2023034 Brookhaven National Laboratory - the participation of
 154 the Czech Republic.

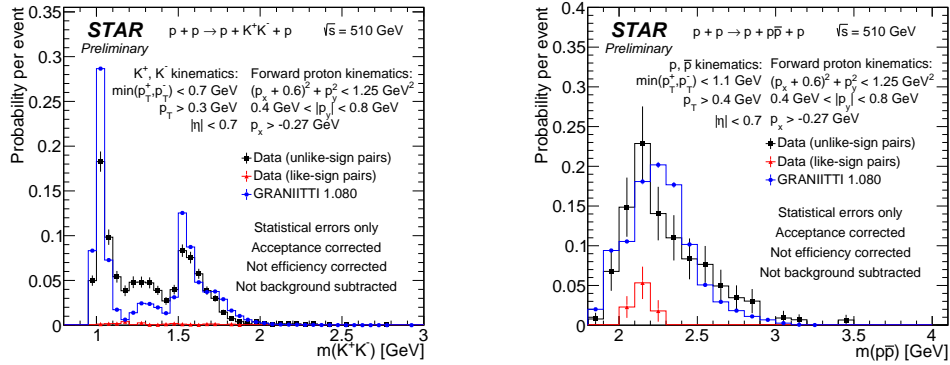


Fig. 4. Acceptance corrected invariant mass spectra of exclusively produced K^+K^- (left) and $p\bar{p}$ (right) pairs at $\sqrt{s} = 510$ GeV. Error bars represent the statistical uncertainties.

REFERENCES

- 155 [1] M. G. Albrow, T.D. Coughlin and J.R. Forshaw, *Prog. Part. Nucl. Phys.* **65**,
 156 149 (2010).
 157 [2] K. Ishikawa, G. Schierholz and M. Teper, *Z. Phys. C* **19**, 327 (1983).
 158 [3] H. Hahn *et al.*, *Nucl. Instrum. Meth.* **499**, 245 (2003).
 159 [4] STAR Collab., (J. Adam *et al.*), *JHEP* **07**, 178 (2020).
 160 [5] STAR Collab., (K.H. Ackermann *et al.*), *Nucl. Instrum. Meth.* **499**, 624 (2003).
 161 [6] M. Anderson *et al.*, *Nucl. Instrum. Meth.* **499**, 659 (2003).
 162 [7] STAR Collab., (J. Wu *et al.*), *J. Phys. G* **34**, 729 (2007).
 163 [8] STAR Collab., (C. A. Whitten *et al.*), *AIP Conf. Proc.* **980**, 1 (2008).
 164 [9] S. Bultmann *et al.*, *Nucl. Instrum. Meth.* **535**, 415 (2004).
 165 [10] M. Mieskolainen, *arXiv:1910.06300*
 166 [11] L. A. Harland-Lang *et al.*, *Eur. Phys. J. C* **74**, 2848 (2014)
 167 [12] R. A. Kycia *et al.*, *Commun. Comput. Phys.* **24**, 860 (2018)
 168 [13] R. Ciesielski and K. Goulios, *PoS* **174**, 301 (2013)